8th U. S. National Combustion Meeting
Organized by the Western States Section of the Combustion Institute
and hosted by the University of Utah
May 19-22, 2013

A Study of Strut Based Flame Holder Combustion Physics: Comparing JP-8, JP-7, and RP-2 Fuels

Yolanda R. Hicks[1] *Jinho Lee*[1] *Randy J. Locke*[2]
Sarah A. Tedder[1] *Robert C. Anderson*[1]

[1] *NASA Glenn Research Center, Cleveland Ohio 44135, USA*
[2]*Vantage Partners, LLC, Brook Park Ohio 44142, USA*

This paper summarizes the experimental observations made of the combustion characteristics exhibited by a High Energy Aerated Technology (HEAT) fuel injector integrated bluff body flame holder (fuel strut) with a 15-degree sweep angle. The experiment was conceived to study the effects fuel type and heat input have on the combustion. Three refined petroleum fuels were used in this work: two jet propellants JP-8 and JP-7; and a rocket propellant RP-2. The JP-7 and RP-2 fuels were heated to simulate the combustor environment and the ensuing combustion characteristics were studied. The fuel heating was also undertaken to simulate the use of fuel as a heat sink for cooling, and to investigate effects that fuel decomposition may have on injector operability. The experimental data for all three fuels showed that this flame holder can be operated over the temperature and pressure range typical for combustion in high-speed propulsion systems.

In this study, we used a variety of imaging techniques to consider the fuel state (i.e. liquid or vapor) and combustion characteristics. Among the techniques used are planar laser scatter (PLS) from fuel drops, planar laser-induced fluorescence (PLIF) of fuel, and chemiluminescence imaging using video and high speed digital photography. The instantaneous images obtained using the laser-based methods and the high speed movies show that transient models are needed to characterize this flow field. Also using these tools, we performed a parametric survey of fuel temperature at fixed inlet air conditions (air temperature 1100°F). We varied the fuel temperature from 77°F to 1000°F while acquiring PLS and PLIF. We observed a change in the fluid structure and the nature of the RP-2 combustion between fuel temperatures of 600°F and 700°F. At these fuel temperatures, the fuel has almost fully changed to vapor.

1. Introduction

An examination of multiple endothermic hydrocarbon (HC) fuels has been undertaken to determine how pre-heating or thermal conditioning affects the physical and chemical properties of these fuels. By simulating the passive heating of fuels used for cooling high speed aircraft structural components and using the pre-heated fuels in a flame tube with fuel injector flame holder hardware, the effect of the pre-heating on several fuel types has been determined. As an element of NASA's Aerospace Fundamental Aeronautics Program (FAP) a research effort has been initiated to develop a re-usable hypersonic vehicle. The propulsion systems of these aircraft would be required to function efficiently over a wide range of operational conditions, including utilizing hydrogen (H_2) as a fuel at speeds exceeding Mach 7. However, technical advantages have been shown for using more traditional HC fuels at speeds between Mach 4 and 7 [Hueter 2002]. The potential benefits of using certain conventional HC fuels over the substantial operability range of these hypersonic powerplants has led to a significant research effort at NASA Glenn Research Center (GRC) to understand the fundamental aspects of using heated, "cracked," kerosene type fuels. The main thrust of this particular study focused on examining those operational engine regimes where it has been deemed possible to use conventional liquid hydrocarbon jet propellants (JP) such as Jet-A, JP-8 and JP-7. JP-7 is the preferred candidate fuel for high speed vehicles since it possesses the best overall endothermic properties of the three HC fuels. The more readily available Jet-A and JP-8 were included in this study because JP-7 is, unfortunately, no longer commercially available. Furthermore, efforts already exist to improve JP-8's overall stability characteristics through the use of additives for elevated temperature applications. Additionally, as part of this study, the performance and the effect of pre-heating on rocket propellants (RP) such as RP-2, which is a viable alternate refined fuel, and has remarkably similar endothermic capabilities to JP-7, was also undertaken.

The fuel injector design is a critical element to any study of the propulsion system. Particular emphasis in these studies is placed on characterizing the impact of adding heat to the fuel. The first phase of this study was undertaken to demonstrate the feasibility of using a High Energy Aerated Technology (HEAT) combined fuel injector flame holder design, built in partnership with the Air Force Research Laboratory (AFRL) and installed in the CE-5 engine research test facility at NASA GRC [Lee et al. 2009]. The HEAT injector is based on a typical injector design that may be used for high speed propulsion applications integrated into a bluff body flame holder. Aeration is added to provide the injector atomization control which is essential in the low fuel temperature combustion environment of the lower flight speeds. This phase of the study established that the HEAT fuel injector strut could function suitably within the sector rig in the NASA test cell at the required test conditions thus allowing progression to the second phase of testing involving fuel pre-heating. During the subsequent phases of testing pre-heating of the various JP and RP-2 fuels was accomplished and the results obtained in this study are presented herein.

2. Methods

2.1 HEAT Injector Hardware

Figures 1, 2 and 3 depict the integrated fuel-injector and flame-holder used in this study. Figure 1 is a photograph showing the assembly. Figure 2 is an illustration that depicts its installation within the facility flame tube hardware. The HEAT injector (strut) is the bluffbody/flameholder and measures 1.25 inches wide by 4.5 inches high and fits into a flow path 5 inches wide by 5 inches high. In addition, a generic aerodynamic fairing on the bluff body houses the fuel and cooling passages. A 15-degree swept angle is incorporated into the strut configuration to insure that the secondary flow-field generated moves the flame away from the strut wall. The strut is fabricated from Inconel 625 to minimize required cooling and to reduce the heat loss in the pilot flame region behind the strut. The injector tips were sized using the experimental data from Lin et al. [2002] Atomization air is introduced into the fuel-air mixing chamber located within the strut through a perforated tube fed from an independent high-pressure air source. The injector configuration tested has a design flow number of 76. This test hardware is mechanically capable of simulating both pilot and primary injection schemes. The pilot injection scheme is simulated using axial fuel injection points located on the rear face of the strut. The primary injection scheme is simulated using the transverse fuel injection sites located on both sides of the flame holder strut body. The current configuration of the HEAT injector is sized to handle liquid fuel flows between 0 and 0.3-lbm/s with fuel pressure ranging from 20 to 270 psia. The six injection point HEAT injector configuration was designed to match fuel flow rate with the available facility airflow. Figure 3 shows streamline traces from a simulation that provides insight into the flow field.

The HEAT injector was operated in a facility historically used for combustor subcomponent testing of fuel injector hardware applicable to subsonic and supersonic commercial flight. That is, typical operation of a flame tube incorporated a research fuel injector or fuel air mixer designed specifically for a gas turbine-based engine cycle, and the facility was designed to provide the high pressures up to 275-psia and inlet temperatures required for the next generation of thermodynamically-efficient, low emissions engine. The facility can run for hours, and many operating points can be simulated in a single run. Another advantage of testing in the facility is that optical and laser-based diagnostics can be used to measure certain parameters and visualize the flow because the flame tube can be optically accessed.

The first iteration of HEAT injector testing used JP-8. Although JP-8 /Jet-A can be used endothermically, as a heat sink [Huang et al. 2004], the fuel was not heated for the test series. Instead, the focus was a demonstration that the injector could successfully be installed into the combustion facility and be operated at points relevant to cycle conditions for hypersonic flight.

Two struts were used in testing, both with the same bluff body design;. however, there are some differences. The first iteration of the HEAT injector was specifically designed to accommodate unheated JP-8 proof-of-concept (facility retrofit and injector flight mapping) tests, and was operated with a greater amount of internal cooling than the successor tests. The exit orifices for the fuel were sized with the room temperature JP-8 testing in mind. The latter tests using JP-7 and RP-2 used resized (enlarged) orifices to accommodate a liquid-vapor mix exiting the strut.

Figure 1 Photograph of the HEAT injector integrated flame holder assembly and mounting flange.

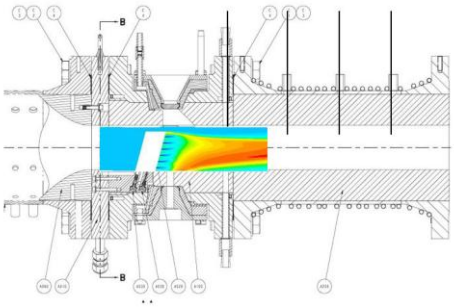

Figure 2 Schematic drawing that shows the placement of the HEAT injector within the optically-accessible combustor assembly for the tests using JP-8 and RP-2. Placement is such that flow over the strut's top and the top two injection points (of six) are visible through window. Flow is left to right.

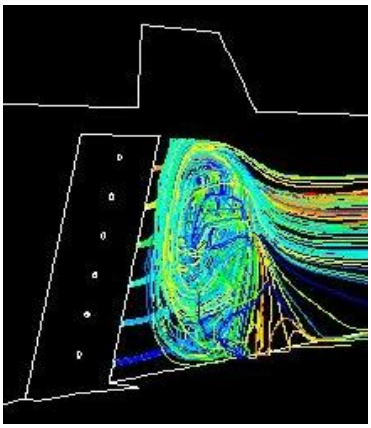

Figure 3 Streamline traces from a simulation showing injected fluid trajectories from HEAT injector. Flow is left to right.

JP-8 is typically the fuel used in the facility, and measurements have been made successfully to determine fuel injector patternation and to assess unmixedness [Hicks et al. 2007; Locke et al. 2003]. Fuel planar laser-induced fluorescence (PLIF) and planar laser scatter (PLS) are used to determine total fuel and liquid fuel fractions, and OH PLIF has been used to assess where primary and secondary combustion reactions occur. We have also measured velocity using particle image velocimetry (PIV) and combustion temperature with spontaneous Raman spectroscopy (SRS), by way of the nitrogen vibrational anti-Stokes/Stokes ratio.

A benefit of using JP-8 is that one can readily obtain fluorescence from the fuel because JP-8 contains up to 19% polycyclic aromatic hydrocarbons (PAH); among those PAH is naphthalene, which is a strong absorber and fluorescer at the UV wavelengths used for fuel PLIF. Using these PAHs has enabled us to use fuel PLIF for in situ fuel injector patternation in realistic combustion environments, and the same excitation wavelength is used to excite OH.

The disadvantage to having the high percentage of aromatic hydrocarbons is the greater tendency to soot at lower temperatures, which is a reason JP-8 is not generally used as a heat sink. JP-8's heat sink capacity is improved by adding a chemical stabilizer to provide for a heat load increase; hence, JP-8 + 100 gives JP-8 an additional 100°F in thermal stability. As noted in the introduction, JP-7 was the endothermic fuel of choice, but is no longer made. However, a study by Huang et al. [2004] determined that the liquid phase differences between JP-8 + 100 and JP-7 are relatively small. Lovestead and Bruno did a distillation study comparing JP-7, RP-1, and RP-2 and calculated the enthalpies. In the study, they showed that JP-7 and the rocket propellants have nearly identical compositional profiles, in terms of the ranges of fuel classes, i.e., paraffins, monocycloparaffins, dicycloparaffins, alkylbenzenes, naphthalenes, and indanes/tetralins. There are some differences in the volatility at different distillation fuel fractions, however. For example, they found JP-7 to be less volatile at lower fuel fractions (of distillate) and more volatile at higher distillation fractions than RP. JP-7 contains approximately 3% alkylbenzenes and 1% naphthalenes. Another distillation study [Ott et al 2008] on the rocket propellants shows that RP-2 contains approximately 3.5% by volume alkylbenzenes and about 0.5% naphthalenes on average, and that the percentages increase slightly with distillate fraction. Exciting the alkylbenzenes for fuel PLIF requires exciting these components at a shorter wavelength than we use for the naphthalenes, and the significantly lower percentage in JP-7 and RP-2 poses an additional measurement challenge.

Thus, the largest difference between the fuels from an optical diagnostics perspective is the amount of fluorescent aromatics contained within the fuels. We have made use of the napthalenes in JP-8, but JP-7 and RP-2 contain much less. Therefore, a part of our study compared excitation/detection schemes for applying fuel PLIF by way of exciting the methylbenzenes for different fuels.

2.2 Experimental Setup—PLIF, PLS, Luminescence

The experimental setups that fall under the category of imaging techniques were similar in that any light scattered or emitted was collected, using an imaging array (camera), from an angle perpendicular to the combustor flow direction, as illustrated in figure 4. Various filters were applied so that only the wavelength bands of interest were allowed to pass to the detector. For PLIF and PLS, the two 2-D laser-based techniques, the laser beam was formed into a light sheet using a set of cylindrical lenses, to obtain a sheet approximately 300 µm thick. The sheet was passed vertically through the test section and aligned parallel with the flow direction. For these methods, the laser sheet and collection optics are traversed together so as to maintain focus on the laser sheet. For chemiluminescence measurements, either species-specific, or high speed imaging, the camera was typically positioned so that the vertical center plane of the test rig was in focus.

PLS and fuel PLIF images, along with chemiluminescence images of C_2, were obtained using the same receiving optics and camera. Collection optics included the appropriate filter (FWHM of 10-nm, typical) attached to a UV-grade, f = 105-mm, f/4.5, macro camera lens. The light was collected using a gated, 16-bit, 1k × 1k pixel array, intensified CCD (ICCD) camera having a Gen II Super-Blue-Slow-Gate intensifier. We collected sets of single-shot images. For PLIF and PLS, we used a camera gate width of 100-ns to 200-ns; for the chemiluminescence images, the exposure was generally set to a gate width of 100µs. With JP-8 as the fuel, we also obtained images by integrating gated events on the detector (on-chip averaging). A 10-Hz, frequency-doubled Nd:YAG-pumped dye laser/frequency mixer system to achieve wavelengths around 282-nm was used to excite fuel molecules of JP-8 and JP-7. A 10-Hz, frequency-tripled Nd:YAG-pumped OPO system served to excite the RP-2 fuel molecules near 274-nm. In all cases, the fuel excitation wavelength was also used in the PLS technique. The laser was formed into a sheet using a pair of cylindrical lenses, to obtain a sheet approximately 300 µm thick. For chemiluminescence, we averaged 600 gates on-chip. The filters used to isolate the species were 280-nm (PLS), 297-nm (fuel), 334-nm (fuel), and 515-nm (C_2).

Flame imaging was achieved using a 12-bit, high speed CMOS camera (1k × 1k) focused on the vertical center plane. The frame rate and resolution are variable. The camera can image as fast as 5400-frames/s (5.4-kps) at full resolution, and faster at lower resolutions. Light emitted from the volume and within the field-of-view of the collection optics was obtained. The flame chemiluminescence was collected using either an f = 200-mm, f/4 lens or an f = 150-mm, f/1.2 lens. The camera array is sensitive to visible light. The light collected was largely a combination of CH and C_2 emissions; alternatively, the flow field was illuminated by the luminous flame downstream of the field-of-view. Keeping in mind available test time, we made an on-the-fly effort to optimize the exposures for the high speed images. Selection of neutral density filters; image exposure times, frame rate, and total image area read out were factors in determining exposure. Whether using the gated ICCD or the CMOS camera, all chemiluminescence images are volume-based, line-of-sight images, meaning that the total intensity recorded comes from the entire combustor volume that is within the field of view.

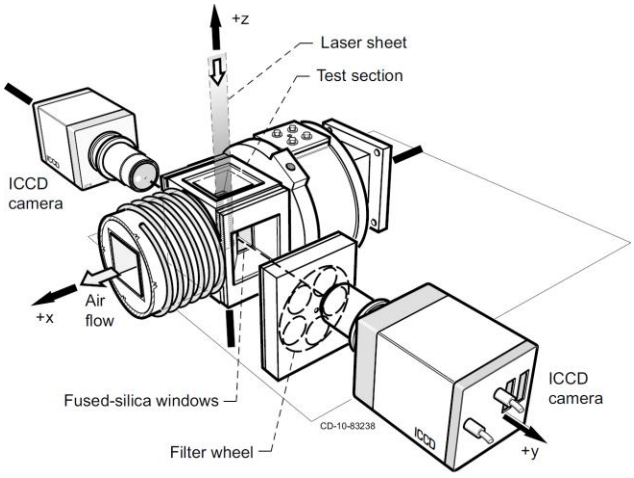

Figure 4 Illustration showing a typical 2D imaging setup

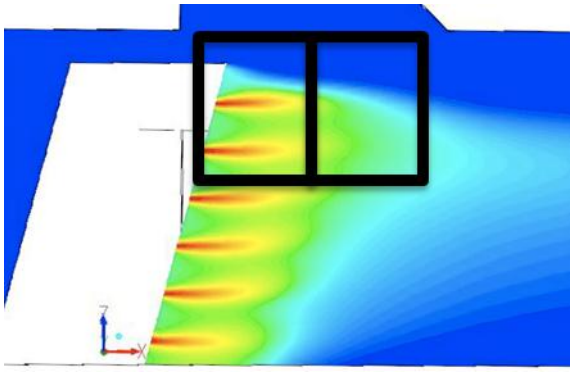

Figure 5 Cartoon showing the window positions (outlined in black with respect to the HEAT injector. Testing with JP-8 and RP-2 position was close to strut exit. For testing with JP-7, the window was 1.5 inches downstream of the strut exit.

Two fields of view were used during testing. For the JP-8 and RP-2-fueled experiments, the strut was set up so that the field immediately downstream from its exit could be seen within the 2-inch high by 1.5 inch wide windows; When JP-7 was used, the strut was installed so that the field roughly 1.5 inches to 3 inches downstream could be interrogated. Figure 5 shows a cartoon that highlights these different fields of view.

3. Results and Discussion

General Overview of the Three Test Series

When running the JP-8-fueled tests, we determined quickly that we would not be able to use our laser-based techniques as planned because PLIF and PLS relied on collecting light 90° from the entry. That is, we insert the laser beam or sheet vertically into the flame tube, and collect through a side window; however, the top window quickly became so dirty that the laser sheet could not penetrate into the combustor, and the PLIF and PLS experiments could not be done. Therefore, aside from a few PLIF and PLS data sets acquired shortly after lighting the combustor, the remaining data were obtained via high speed imaging and with standard video imaging, which used only the side windows.

Because JP-7 is no longer made, testing was conducted using a limited supply of available fuel. Also, since the first series using JP-8 immediately fouled the top window, we chose to obtain data downstream of the strut injection sites and shifted the field of view 1.5 inches, which is the axial extent of the window. Therefore, there is no overlap in field of view with the upstream position used during the first test series using JP-8. We acquired images of fuel PLIF, PLS, and chemilumenescence of C_2. We also used high speed imaging and standard video imaging with this configuration. The top window generally stayed clean, although on occasion material deposited on the window and caused obscuration of the laser sheet in certain spots, essentially creating a shadow effect, which can be seen as vertical streaks in the resulting images. During these JP-7 tests, most of the data were acquired with the fuel heated to 900°F at the injector.

During the final test series, using RP-2 with the field-of-view in the upstream position, we expected to run the full suite of experiments originally planned, including temperature measurements via Raman scattering. However, a critical valve for the fuel heater system failed, resulting in a premature end to the optical testing with RP-2. We were able to acquire limited PLIF and PLS data to characterize the system during the fuel heating cycle, and we also obtained high speed images and video. The window location was as for JP-8, immediately downstream of the strut. The top window stayed clean during the time we tested, approximately 2.5 hours.

For the cases of JP-8 and RP-2, we saw strong evidence of optical thickness in that the laser energy was strongly absorbed and/or scattered by the fuel from the top jet, leaving very little to interact with the second jet. There were also signs of optical thickness when using JP-7 because we observed less signal in the lower jet stream. We know the fuel flow was nominally the same in both jets because they appear to have similar intensity in the high speed images. The JP-8 system was the most optically-thick, primarily because it consisted of the largest percentage of absorbing constituent species—aromatics (naphthalenes in particular). JP-8 contains up to 20% aromatics by volume, compared to 4% for JP-7 and RP-2. Although the percentage of aromatics is much lower for the latter fuels and is predominantly methyl-benzenes, the high fuel flow rates present a large number of absorbers, which again, leave little available light for the second fuel jet. For this reason, we focus on the top jet for the laser-based results presented in this report.

One other factor that influenced our ability to capture details of the two jets within the field of view was the growth of soot that adhered to the rear face of the strut, as illustrated in figure 6, which shows frames from the high speed camera during testing with RP-2. The left hand image of figure 6 shows the combustion environment without soot on the HEAT injector (its tip can be seen in the upper left corner, as in figure 5). In the image on the right, deposits obscure approximately 40% of the image. The soot growth occurred with and without aeration, and seemed to require a certain critical mass before it would blow off. The soot had the primary effect of obscuring the field of view, certainly for light collection, and possibly preventing the laser sheet from passing through the flow field. Secondarily, it may also have affected the normal progression of the fuel jet, though we had no means to assess this possibility. Given that our PLS and fuel PLIF signals were relatively high during the JP-7 tests when the optical access was downstream, it is likely that small particles of soot were carried downstream with the fuel jet. Since the naphthalenes and methyl-benzenes we target for fuel PLIF can also be characterized as soot precursors, any soot carried downstream would also fluoresce and scatter light.

Specific Details and Comparison of Results

Figure 7 shows the laser-based results obtained during the tests with JP-8, as well as a C_2 chemiluminescence image and a single high speed image frame. Flow is from left to right. All data were acquired with air flow of 4.5 lb_m/s at T_3 = 980°F, P_3 = 90 psia, and 1.4% combustor pressure drop, and fuel temperature of 55°F with flow of 277 lb_m/h and 14-psi pressure drop. The top row shows the average scattered light signal from 100 single laser shots (camera gate time = 100-ns) on the left, and the corresponding PLS image acquired by integrating on-chip 100 gates. In comparing the single shot average with the accumulated average, we see that the fields appear very similar. The key differences are that in the on-chip average, more of the available camera dynamic range is used, and better signal-to-noise ratio is achieved, but it tends to wash out individual instances of where fuel droplets are located, which can be seen in the average of single shots. In general, both images show that some liquid fuel becomes entrained in the region of shear that develops as the air passes over the strut. All that can be seen of the top jet is a few large droplets downstream (single-shot average). The second row of images is of fuel PLIF. Again, the left image consists of a single shot average of 100 images, while the right image is an on-chip average of 600 gates. As with the PLS, the single shot average can best represent the overall system average, but the on-chip has much better signal-to-noise. These images show primarily the entrained fuel layer carried within the shear layer, and little can be seen of the top fuel jet, and nothing at all from the second fuel stream. The bottom row of figures shows chemiluminescence from the flame. On the left is a frame from the high speed camera framed at 2-kHz, with an exposure time of 500-µs. This image is illuminated more by the light given off by downstream burning than by chemical bond-breakage (self-luminance) of the fuel jets themselves. Note that both fuel jets can be seen clearly in the image, as well as the shear layer that passes above the strut. The image on the right results from chemiluminescence from C_2, an on-chip average of 600 gates. Both fuel jets can also be seen in this image, though not as clearly as for the high speed image. The C_2 image has similar features to the PLS and PLIF in that the shear layer can be seen, but it also shows that chemical reactions are occurring in the near field layer close to the strut and in the top jet, but the second jet has not yet begun reacting within the field of view. The other feature one can see is soot growth has begun to form on the strut. Retrospectively, we can see that this soot build-up also is in the fuel PLIF on-chip average. The movie frame was acquired near the beginning of a different test day, and does not show soot growth.

The shear region that passes downward across the top of the strut was evident in the tests with JP-8 and also appears in the tests that used RP-2 as the fuel. This is an expected feature of the design, and matches simulations, such as the temperature field overlay shown in figure 2 and the particle trajectories in the simulation result shown in figure 3. The shear region can be seen in figures 8 and 9, which show how the fuel PLIF and PLS signals are affected as a function of RP-2 fuel temperature only. The air inlet conditions are 1100°F, 68-psia, 4.5 lb_m/s and 1.4% pressure drop, and the fuel flow rate was 277 lb_m/h. Each image is comprised of the average of 100 single images, acquired at a rate of 10-Hz. Variance in temperature was at most 10°F. (The fuel temperature ramp rate is normally 100°/min.)

As noted earlier, the system is optically thick, so much of the initial laser energy, which is reduced due to absorption and/or scatter by molecules as it travels through the combustor, is substantially lower by the time it reaches the region of the second fuel jet. For the lowest three fuel inlet temperatures shown in the PLS images (figure 8), the lower fuel jet can be seen, but with much lower signal. As the fuel temperature rises beyond 300°F, little to no signal remains for the lower jet, and the signal from the top jet dissipates, which allows the signal from the shear region to be more prominent. The same trends hold for the PLIF images in figure 9, though the fluorescence signal is much lower.

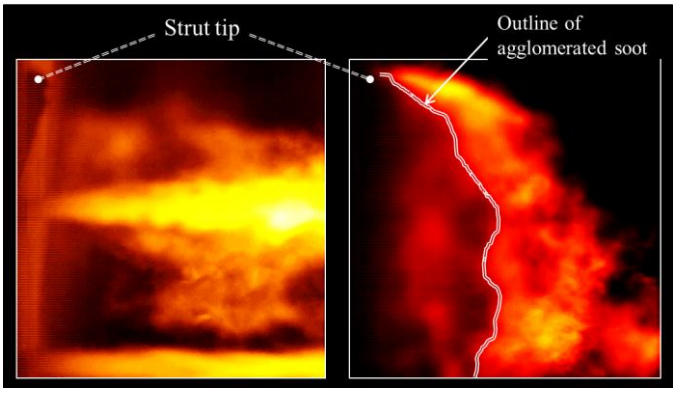

Figure 6 Example that shows RP-2 combustion field without left) and with (right) an agglomeration of soot affixed to the rear face of the strut. Flow is left to right.

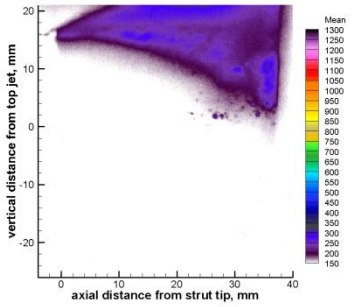

Planar Laser Scatter, Average of 100 single shots

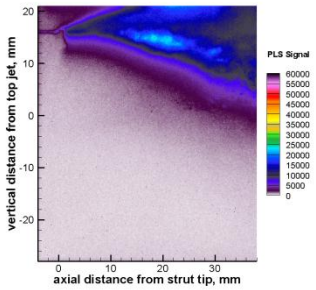

Planar Laser Scatter, 100 shots accumulated on-chip

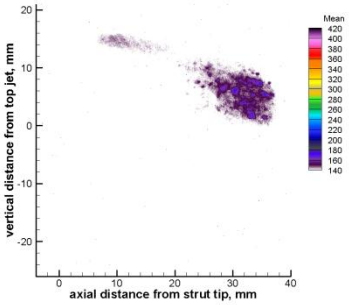

Fuel PLIF, Average of 100 single shots

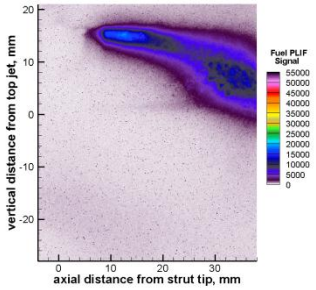

Fuel PLIF, 600 shots accumulated on-chip

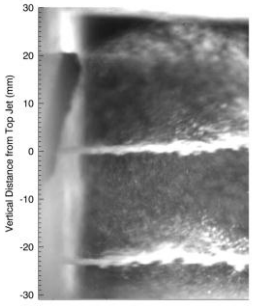

Single frame from High Speed camera. Frame rate = 2 kHz, exposure time = 500 µs.

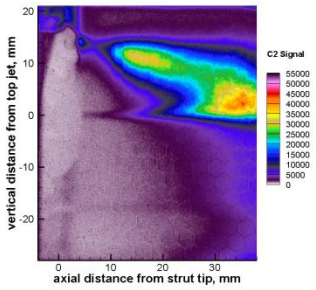

C_2 chemiluminescence, 600 gates of 100-ns, accumulated on-chip

Figure 7 JP-8 Results: Images of PLS (top row), fuel PLIF (middle row), along with a high speed camera image (bottom left) and C_2 chemiluminescence (bottom right). Flow is left to right. Inlet conditions: air at 4.5 lb_m/s at T_3 = 980°F, P_3 = 90 psia, and 1.4% $\Delta P/P_3$, and fuel temperature was 55°F with flow of 277 lb_m/h and 14psid

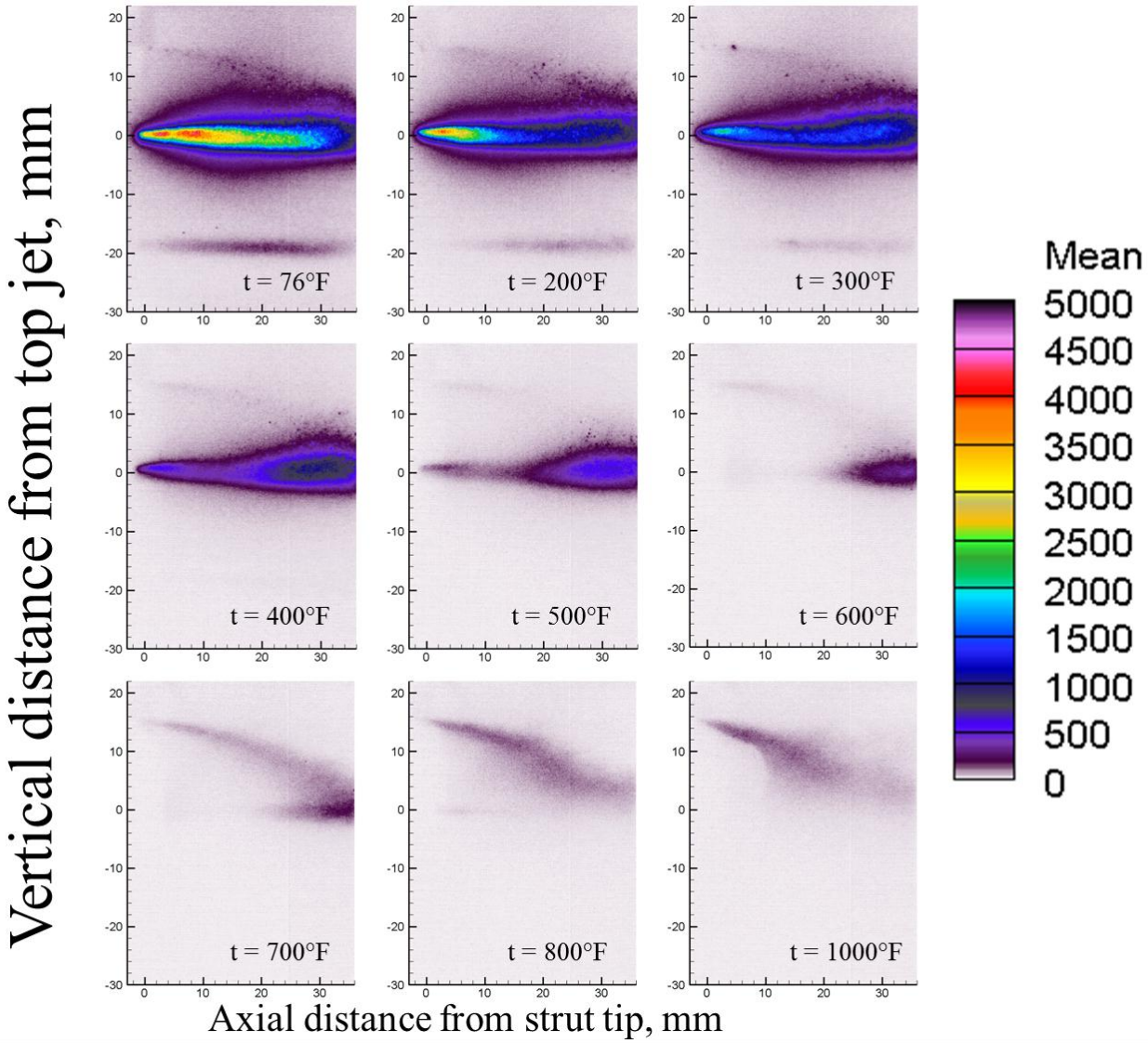

Figure 8 Mean signal acquired from 100 single shot PLS images for nine different inlet RP-2 fuel temperatures. The air inlet conditions are 1100°F, 68-psia, 4.5 lb_m/s and 1.4% pressure drop, and the fuel flow rate was 277 lb_m/h. All images are plotted on the same scale. Flow is left to right.

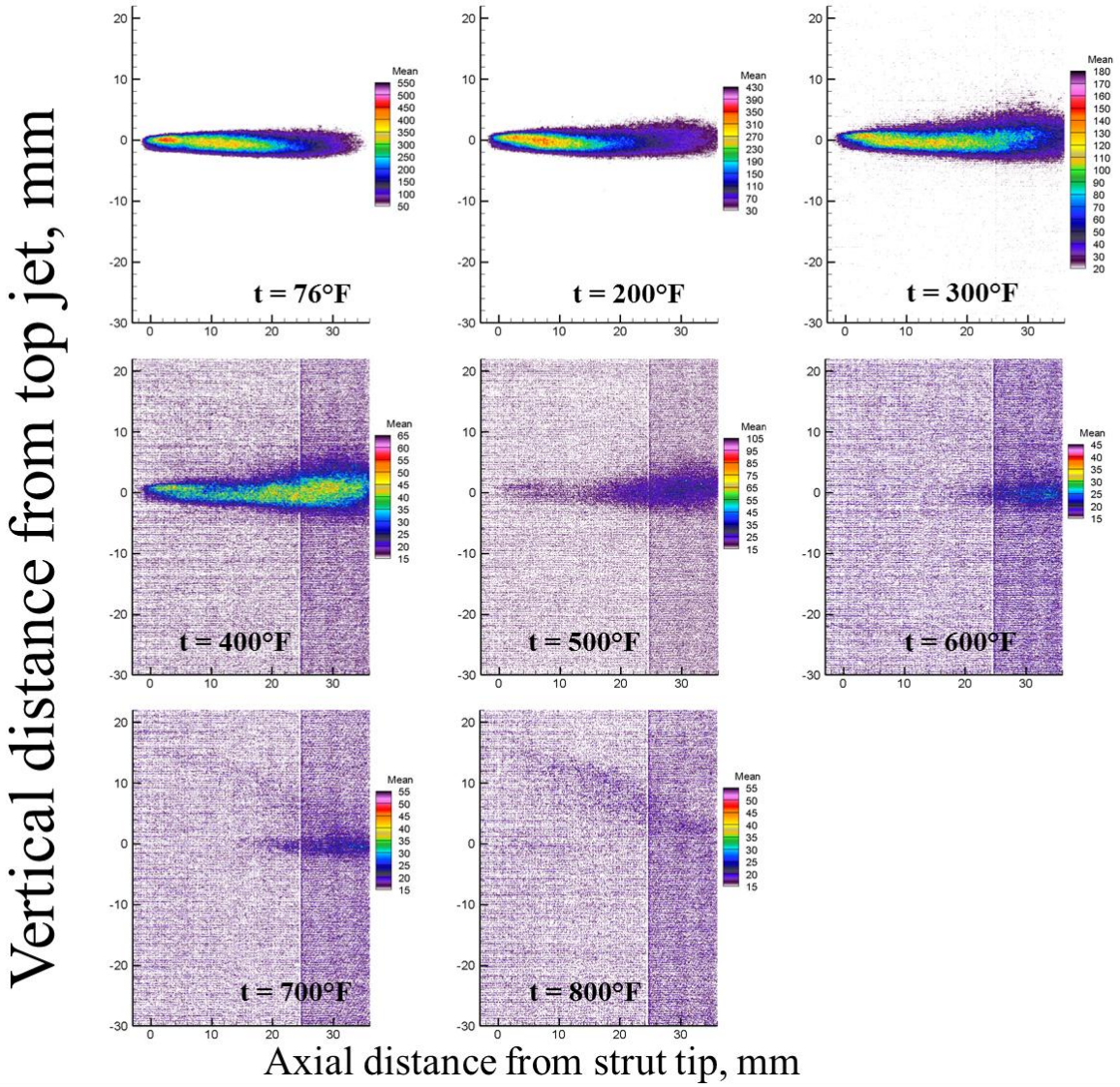

Figure 9 Fuel PLIF (297nm) mean signal acquired from 100 single-shot images for eight different inlet RP-2 fuel temperatures. Flow is left to right. The PLIF signal with fuel temperature 1000°F was indistinguishable from the background and not included here. The air inlet conditions are 1100°F, 68-psia, 4.5 lb_m/s and 1.4% pressure drop, and the fuel flow rate was 277-lb_m/h.

Figure 10 shows plots of the normalized mean maximum signals for PLIF and PLS on the y-axis as a function of fuel inlet temperature on the x-axis. The mean values were obtained by first calculating on a per-pixel basis the maximum average signal from the sets of 100 single-shot images, then computing the average signal value within the region of interest. Similarly, the RMS values were calculated by averaging the per-pixel RMS values. We chose the means of the maxima to plot rather than the true mean because this places emphasis on the largest drops and/or a larger droplet number density. The region of interest contains the top jet and extends approximately 40-mm axially and 25-mm above and below. The error bars represent the mean standard error (standard deviation divided by square root of sample size) of the 100 images obtained at each fuel temperature. The PLIF signal has more error, primarily because the fluorescence signal was quite low on a shot-to-shot basis. We chose 100 single-shots in the interest of time, but would have been better served to collect more images. Both plots show decay in signal with increase in fuel temperature, and with similar rates. The PLIF signal falls to 10% of the maximum by T = 400°F and to 0 by 600°F, whereas the PLS signal falls to 10% at approximately 750°F and to 0 by 800°F.

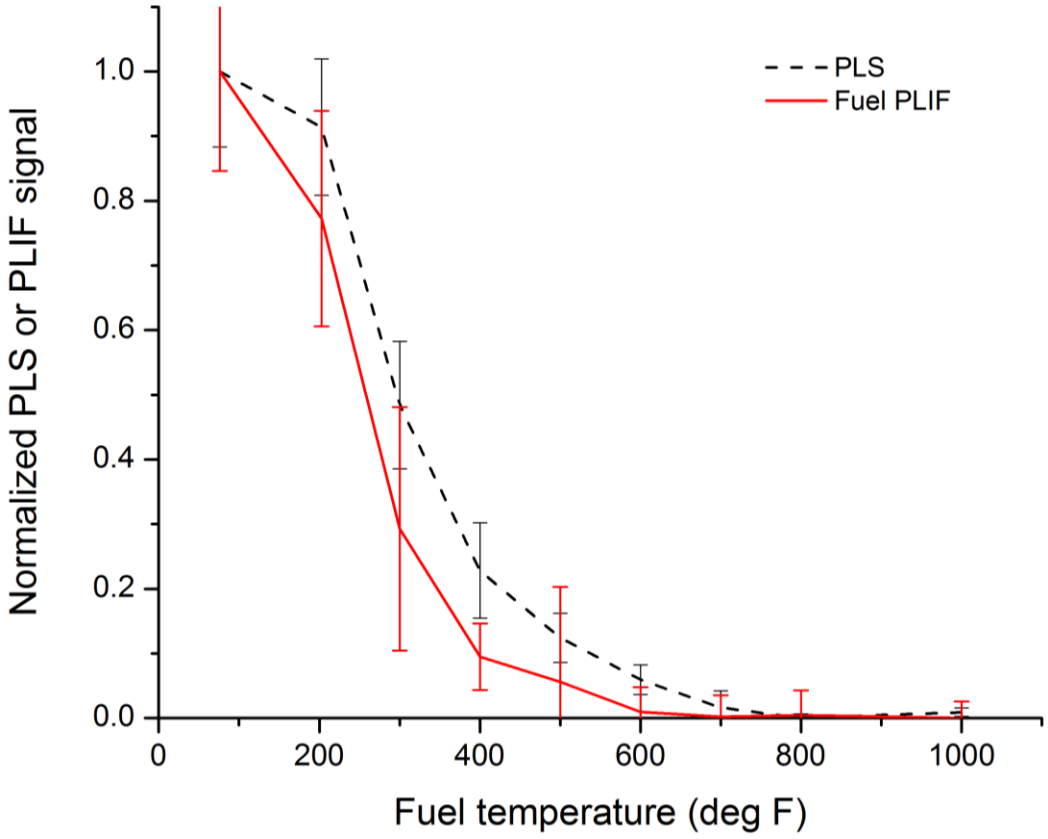

Figure 10 Graph of the normalized fuel PLIF and PLS signals as a function of RP-2 fuel inlet temperature. Plots show the mean of the maximum signal encountered for each of the 100 images within a region ± 25-mm about the top fuel jet. Both plots show decay in signal with increase in fuel temperature, and with similar rate; however fuel PLIF is likely to decay faster because the fluorescence yield decreases with increasing fuel temperature. The PLIF signal falls to 10% of the maximum by T = 400°F and to 0 by 600°F, whereas the PLS signal falls to 10% at approximately 750°F and to 0 by 800°F.

Because the JP-7 images were acquired downstream, and for expedience, only at a few selected points to map out a flight trajectory (up to Mach 4), a direct comparison for all three fuels could not be made. However, given the similarities we see between JP-8 and RP-2, such as similar fluidic structures and growth of soot on the strut, and the knowledge that the three fuels are more similar than dissimilar [Lovestead and Bruno 2009; Ott et al. 2008], we expect JP-7 in the upstream position would appear similar to the RP-2 images. Likewise, the JP-7 images are a fair representation of what would appear downstream for RP-2 and a heated JP-8 or JP-8+100 system.

Figures 11 and 12 show high speed images from the RP-2- and JP-7-fueled combustors. In figure 11, the left column shows single images of RP-2 at 200°F, 600°F, and 800°F, in an 1100°F airstream flowing 4.5lbm/s at 90-psi. The field of view is the upstream view, in which the strut tip is in the image (upper left). The fuel jets, which can be seen clearly at the low fuel temperature, are barely visible at 600°F, and are not distinguishable at 800°F. The right column shows images using JP-7, with the field-of-view shifted downstream by 1.5 inches. The air inlet conditions were 650°F, 55-psia, 5.4 lb_m/s and 3.5% pressure drop, and the fuel flow rate was 692 lb_m/h. The fuel temperature was 640°F, but the fuel jets can be readily seen two inches downstream of the strut; when the fuel temperature is 900°F, the fuel jets can no longer be distinguished. The JP-7 inlet conditions were quite different from those used for

Figure 12 shows a series of ten consecutive high speed camera frames during JP-7 combustion at air conditions similar to those for the RP-2-fueled system. The frame rate was 10,800 frames/s, and the exposure time was 92.5 µs. This frame rate enabled us to have a pixel resolution such that we captured the entire window field of view. The air inlet conditions are 1000°F, 90-psia, 4.5 lb_m/s and 1.4% pressure drop, and the fuel flow rate was 497 lb_m/h. The images show the "instantaneous" variations in flow, but the frame rate in this case is fast enough that one can track some features frame to frame. Unlike the images of the combustion system under lower fuel temperature (figures 11 or 13), in which the luminous field occupies just the lower half of the images, these images show the luminous structure filling most of the field of view.

RP-2, fuel temperature = 200°F

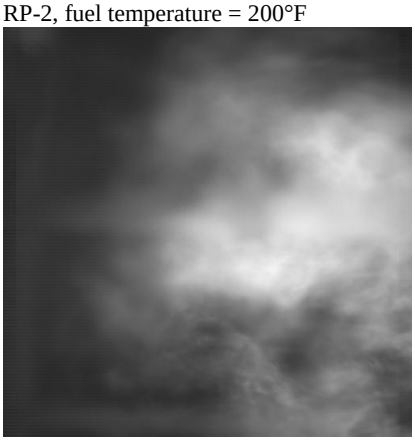

RP-2, fuel temperature = 600°F

JP-7, fuel temperature = 640°F

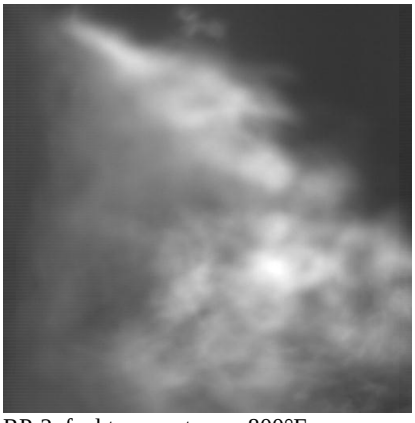

RP-2, fuel temperature = 800°F

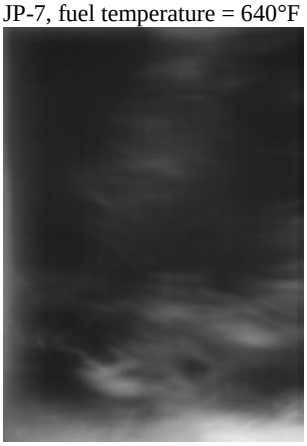

JP-7, fuel temperature = 900°F

Air inlet conditions are 1100°F, 90-psia, 4.5 lb_m/s and 1.4% pressure drop, and the fuel flow rate 277 lb_m/h. The frame rate for all RP-2 images was 20-kHz, with exposure time = 50µs.

Air inlet conditions are 650°F, 55-psia, 5.4 lb_m/s and 3.5% pressure drop, and the fuel flow rate 692 lb_m/h. The frame rate for the top image was 21.6-kHz, exposure time 46.3µs; for bottom was 10.8-kHz, with exposure time 92.6µs.

Fig 11 Single frames from the high speed camera for RP-2 (left) and JP-7 at the fuel temperatures noted with each image. The RP2-fueled system has a field-of-view in the upstream position, with the strut tip visible in the upper left (200°F). The JP7-fueled system field of view is positioned so that the upstream edge (left) is approximately 38-mm downstream of the strut tip. Flow is left to right.

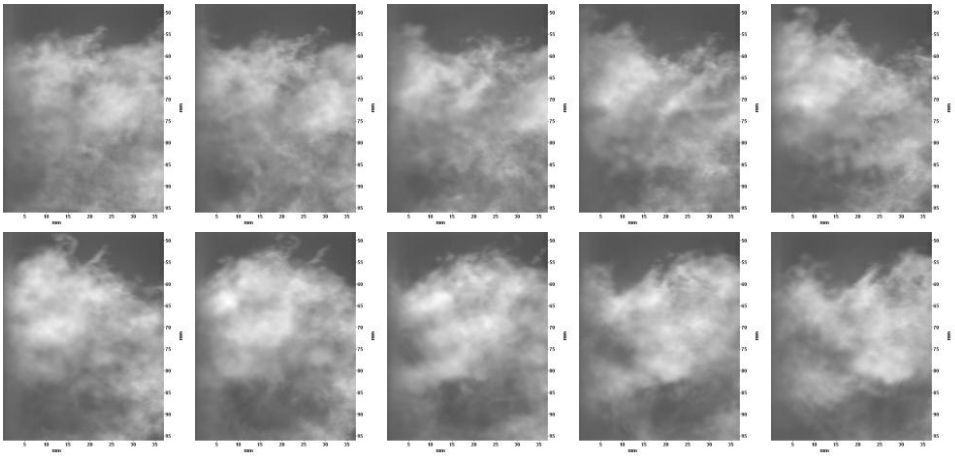

Figure 12 Ten consecutive high speed camera frames of RP-2 combustion, framed at a rate of 10,800/s. Flow is left to right. The field of view begins approximately 1.5 inches downstream of the strut. The air inlet conditions are 1000°F, 90-psia, 4.5 lb_m/s and 1.4% pressure drop, and the fuel flow rate was 497 lb_m/h and fuel temperature was 900°F.

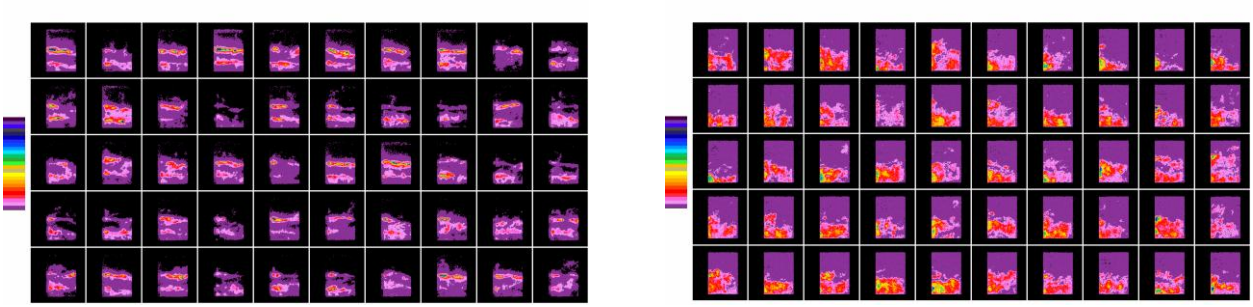

Fuel temperature = 640°F Fuel temperature = 900°F

Figure 13 Fifty single shot frames (of 300), fluorescence from JP-7 fuel jets. Each image is scaled independently. Flow is left to right. The air inlet conditions are 650°F, 55-psia, 5.4 lb_m/s and 3.5% pressure drop, and the fuel flow rate was 692 lb_m/h. The fuel temperatures are as noted with each image.

Table 1 Summary table comparing statistical values obtained using low temperature and high temperature RP-2 fuel.

	Low fuel temperature	High fuel temperature
Mean, counts	1236	741
Median, counts	1005	709
Standard deviation	738	134
Signal span (high – low), counts	5648	842
Standard error	42	7.7
Kurtosis	17	6
Skewness	3	2

Once the fuel becomes fully heated (to 900°F in this case), the coherent jet structure is reduced or eliminated altogether, which we see in the single-shot images, and is highlighted in the composite statistical images shown in figure 14, which shows the mean, standard deviation, and signal spans derived on a pixel-by-pixel basis for 300 single-shot images acquired at the high and low fuel temperature settings for JP-7. In table 1, we also provide the statistics for the

area that encompasses the bulk of the signal at both fuel temperatures, calculated as described above. The region of interest in this case spanned the full axial range and covered the vertical area from 0 to 40-mm. The mean signal is larger for the colder fuel temperature, as expected.

In figure 15, we present the average chemiluminescence signal obtained by processing the individual frames from the high speed camera (pixel-by-pixel), obtained during the fuel temperature survey. Flow is from left to right. The air inlet conditions are 1100°F, 90-psia, 4.5-lb_m/s and 1.4% pressure drop, and the fuel flow rate was 277-lb_m/h. The images were all acquired using 20000 frames/s. The image exposure times were 50-µs for fuel temperatures 600°F and below, and 28.6µs for higher fuel temperatures. The signal intensity has been corrected for the different exposure times. At lower fuel temperatures, we see a mostly intact jet, with some signs of expansion, and that some chemical reaction has occurred. At 400°F, the jet has expanded more, and the signal intensity has increased. By 600°F, the jet has been almost completely obscured the high light levels given off by C_2 and CH bond breakage. As the fuel temperature continues to increase, the onset of burning occurs closer to the injector, evidenced by the higher and higher upstream signal, as the fuel is heated. One can observe an anomaly for the highest three fuel temperatures, which are due to the growth of soot on the injector face. The soot deposit is most apparent in the 700°F case, and by 800°F, some of that soot was removed (swept downstream); however, by the time the fuel temperature reached 1000°F, more soot was added.

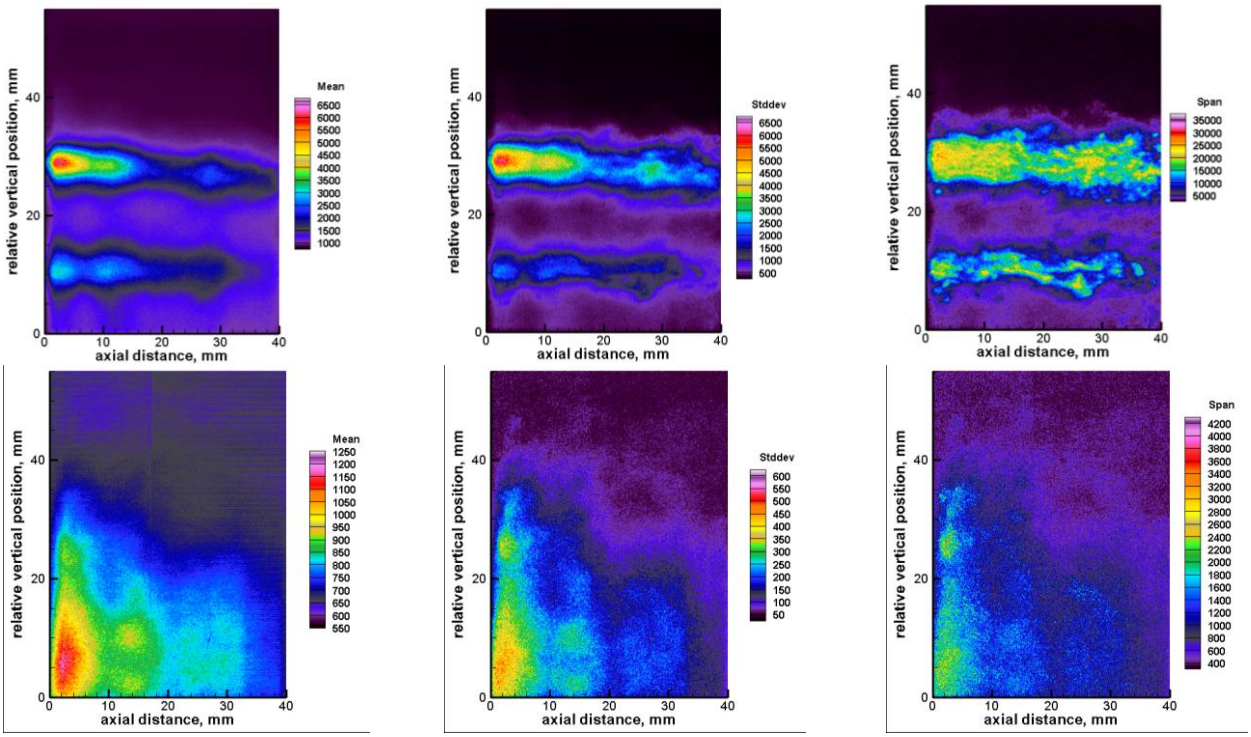

Figure 14 Mean, standard deviation and signal span (maximum – minimum) computed pixel-by-pixel for the 300 image sets highlighted in figure 13. Flow is left to right. Top row: fuel temperature = 640°F. Bottom row: fuel temperature = 900°F.

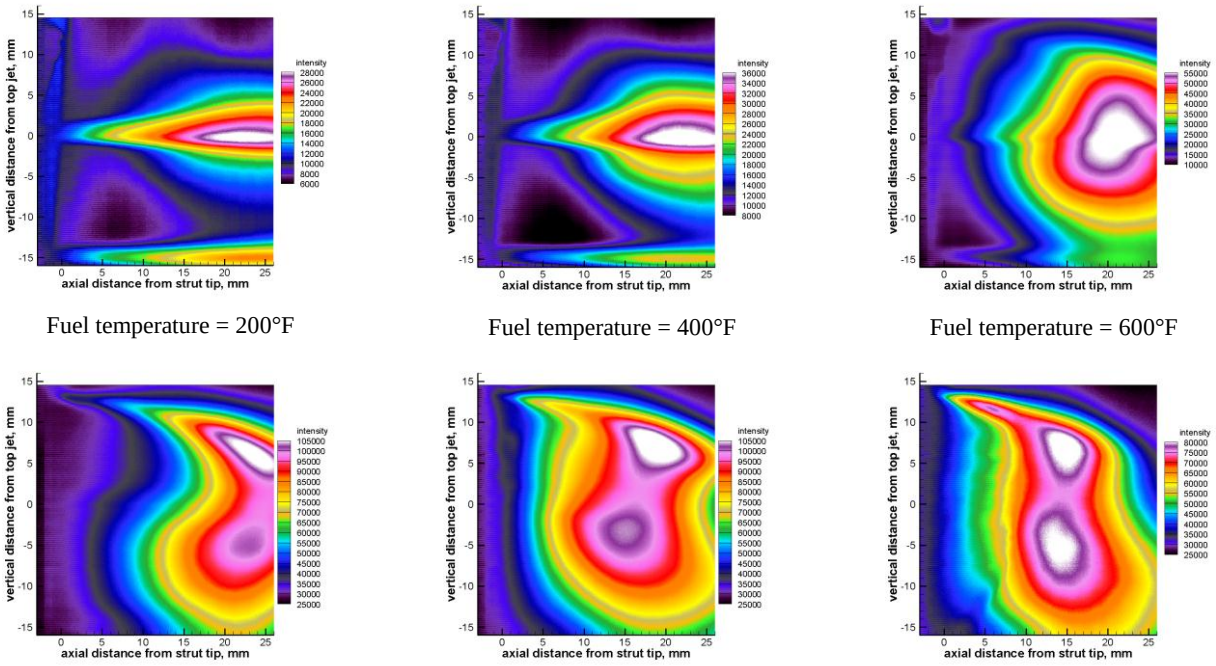

Fuel temperature = 200°F | Fuel temperature = 400°F | Fuel temperature = 600°F

Fuel temperature = 700°F | Fuel temperature = 800°F | Fuel temperature = 1000°F

Figure 15 Images of average flame structure and luminous intensity at selected RP-2 fuel temperatures, obtained by averaging individual high speed camera frames. Each image is independently scaled, with intensity values corrected by image exposure time. The frame rate was 20000/s. Flow is left to right. The air inlet conditions are 1100°F, 90-psia, 4.5 lb_m/s and 1.4% pressure drop, and the fuel flow rate was 277 lb_m/h.

4. Conclusions

We have presented data from the HEAT injector operating with JP-8, JP-7, and RP-2 fuels, which shows the effect of heating the fuel on combustion performance, via optical diagnostic methods. Fuel temperatures varied from ambient to 1000°F. This experiment simulated the combustor environment of a generic turbine based combined cycle engine operating up to a Mach 4 flight conditions.

A fuel temperature survey using RP-2 showed that the fuel PLIF signal falls to 10% of the maximum by the time the fuel temperature reaches 400°F and drops further down to 0% by fuel temperature is raised to 600°F. Similarly the PLS signal falls to 10% when the fuel temperature reaches 750°F and drops further to 0 by fuel temperature is raised to 800°F. The chemiluminescence imaging results were consistent with these observations. We also saw that as the fuel temperature increases, the reaction zone moves upstream, closer to the injector.

We noted that for understanding the flow fields formed by the HEAT injector, the fuels used would likely provide similar results. The difference in applying fuel PLIF will be whether to focus on naphthalenes (JP-8) or methylbenzenes (RP-1 or RP-2). For future research using the HEAT injector, we recommend attempting intermittent bursts of a higher level of aeration to remove the soot growth on the injector to improve the optical properties of the flow observed. If the rear face of the strut can be kept adequately clean, implementing PLIF and PLS—as was done in this work—and particle image velocimetry and Raman spectroscopy for temperature measurements can be readily achieved. Raman spectroscopy would be especially attractive at the higher fuel temperatures. We saw also that the side windows stayed clean, so techniques such as absorption for species or temperature measurements, and laser Doppler interferometry for drop sizing and velocity, might also be viable techniques.

Acknowledgements

This research was funded by the NASA Fundamental Aeronautics Hypersonics and Aeronautical Sciences Projects. The authors also acknowledge the help of the engineers and technicians at the NASA GRC combustor subcomponent test facility: D. Podboy, T. Barkis, W. Rozman, H. Redloske.

References

Y.R. Hicks, R.J. Locke, R.C. Anderson [2007]. Optical Measurements in a Combustor Using a 9-Point Swirl-Venturi Fuel Injector, Paper ISABE 2007-1280.

H. Huang, L.J. Spadaccini, and D.R. Sobel [2004]. Fuel-Cooled Thermal Management for Advanced Aeroengines, *Transactions of the ASME*, Vol 126, April.

U. Hueter, C.R. McClinton [2002]. NASA's Advanced Space Transportation Hypersonic Program, AIAA Paper 2002-5175, 2002.

J. Lee, Y.R. Hicks, R.J. Locke, C.Wey [2009]. A study of strut based flame holder combustion physics: an initial characterization study using Jet-A, presented at 6th National U.S. Combustion Meeting, Ann Arbor MI, May.

K.C. Lin, P.J. Kennedy, T.A. Jackson [2002]. Penetration Height of Liquid Jets in High Speed Cross Flows, Paper AIAA-2002-0873.

R.J. Locke, Y.R. Hicks, R.C. Anderson [2003], in: C. Mercer (Ed.), Optical Metrology for Fluids, Combustion, and Solids, Kluwer Academic Publishers, pp. 175-208.

T.M. Lovestead, and T.J. Bruno [2009]. A Comparison of the Hypersonic Vehicle Fuel JP-7 to the Rocket Propellants RP-1 and RP-2 with the Advanced Distillation Curve Method, *Energy and Fuels*, Vol 23 ,pp.3637-3644, June.

L.S. Ott, A.B. Hadler, and T.J. Bruno [2008]. Variability of the Rocket Propellants RP-1, RP-2, and TS-5: Application of a Composition- and Enthalpy-Explicit Distillation Curve Method, *Ind. Eng. Chem.Res.* Vol 47, pp. 9225-9233, October.

J.A. Widegren, and T.J. Bruno [2011]. Thermal Decomposition Kinetics of Kerosene-Based Rocket Propellands. 3. RP-2 with Varying Concentrations of the Stabilizing Additive 1,2,3,4-Tetrahydroquinoline, *Energy and Fuels*, Vol 25, pp. 288-292.